Analysis and Optimization of Energy Variations in MMCs With Variable DC Voltages

Zhengxuan Li, *Student Member, IEEE*, Qiang Song, *Senior Member, IEEE*, Shukai Xu, *Senior Member, IEEE*, Biao Zhao, *Senior Member, IEEE*, Zhanqing Yu, *Member, IEEE*, and Rong Zeng, *Senior Member, IEEE*

***Abstract*—The modular multilevel converter (MMC) containing full-bridge submodules (FBSMs) can increase the modulation index to reduce the energy storage requirement. The MMCs containing FBSMs can also adjust the dc voltage to fit special applications. However, limited research explores the energy storage characteristics of MMCs with variable dc voltages, and few effective approaches can ensure low-energy storage requirements. This study proposes an approximate analysis method for the energy storage requirement in MMC with variable dc voltages. Results reveal that the energy variation under low dc voltages restricts the reduction effects of the increased modulation index on the energy storage requirement. Then, on the basis of the fact that the low ac component of the arm current under low dc voltages provides a large current margin, an optimal circulating current (OCC) is proposed to optimize the energy variation under low dc voltages. In addition, a practical curve-fitting approach is proposed to facilitate the calculation of OCC in real-time controllers. With these approaches, the energy storage requirement with variable dc voltage becomes similar to that with constant rated dc voltage. Simulation and experimental results verify the analysis.**

***Index Terms*—Circulating current, energy storage requirement, energy variation, modular multilevel converter (MMC), variable dc voltage.**

I. Introduction

MODULAR multilevel converters (MMCs) have been widely applied to high-voltage dc (HVdc) projects [1]–[3] because of their advantages, which include modular design, multiple levels, low harmonics, and low power losses [4], [5]. However, given the energy variations in the converter arms, MMCs require large submodule (SM) capacitors to provide sufficient energy storage, such that the capacitor voltage ripple is limited to an acceptable level. For the SM, the capacitor occupies over half of the volume and entails approximately 30% of the cost [6], [7]. As such, suppressing the energy variation and thereby reducing the capacitance have become urgent issues.

One of the common approaches to reduce the energy storage requirement of conventional MMCs based on half-bridge SMs (HBSM) is the active control of the double-frequency circulating current [8]–[11], which is used to suppress the energy variation and capacitor voltage ripples. However, as revealed in [10], the double-frequency circulating current required to suppress the capacitor voltage ripple increases the peak and the root-mean-square (RMS) values of arm current. The necessary current margin under rated power only allows for a limited circulating current. Therefore, the effect of the double-frequency circulating current on the reduction of energy storage requirement is also limited in conventional HBSM-based MMCs.

Recently, the amplitude of the fundamental-frequency component of the energy variation is noted to decrease as the modulation index increases [12]–[14]. Therefore, increasing the modulation index to a specific value can effectively reduce the energy storage requirement. For instance, at a modulation index of $\sqrt{2}$, the energy storage requirement can be reduced by 70% at unity power factor [12], [13]. At nonunity power factors, a reduction can be achieved by also injecting an auxiliary circulating current [14]. The modulation index can be increased by using the full-bridge SMs (FBSMs), which have negative voltage capability. A variant of FBSM called unidirectional current FBSM (UC-FBSM), also with negative voltage capability, was developed to reduce the usage of semiconductors [15], [16].

Another advantage of the MMCs containing FBSMs or UC-FBSMs is the wide-range adjustable dc voltage. The FBSM and UC-FBSM can output negative voltages. Therefore, the difference of the upper and lower arm voltages in an MMC that contains FBSMs or UC-FBSMs cannot be affected even if the sum of them decreases. This means that the FBSM-based MMCs (FB-MMCs), hybrid MMCs that consist of FBSMs and HBSMs (HYB-MMCs), and UC-FBSM-based MMCs (UC-FB-MMCs) can have a wide-range adjustable dc voltages while their ac voltage capabilities are not affected. This feature enables the FB-MMCs, the HYB-MMCs, and the UC-FB-MMCs to fit many applications. For instance, in the Kunliulong HVdc project, China, each pole is composed of several series-connected MMCs that can be smoothly switched in or out online by increasing the dc voltage from 0 to the rated value or decreasing it from the rated value to zero, without affecting the operation of other parts in the system [1], [17], [18]. In the proposal of active dc-fault clearing, the MMCs keep operating after detecting the dc fault

Manuscript received 15 December 2021; revised 16 March 2022 and 12 May 2022; accepted 22 June 2022. Date of publication 28 June 2022; date of current version 6 September 2022. This work was supported by the National Natural Science Foundation of China under Grant 51977119. Recommended for publication by Associate Editor A. Yazdani. *(Corresponding author: Qiang Song.)*

Zhengxuan Li, Qiang Song, Biao Zhao, Zhanqing Yu, and Rong Zeng are with the Department of Electrical Engineering, Tsinghua University, Beijing 100084, China (e-mail: zx-li18@mails.tsinghua.edu.cn; songqiang@tsinghua.edu.cn; zhao-biao@tsinghua.edu.cn; yzq@tsinghua.edu.cn; zengrong@tsinghua.edu.cn).

Shukai Xu is with the Innovation Department, China Southern Power Grid, Guangzhou 510663, China (e-mail: xusk@csg.cn).

Color versions of one or more figures in this article are available at https://doi.org/10.1109/TPEL.2022.3186875.

Digital Object Identifier 10.1109/TPEL.2022.3186875

and quickly reduce the dc voltage from the rated value to zero to actively clear the dc faults [19]–[21]. In the hybrid HVdc that consists of a line-commutated converter (LCC) and an MMC [17], [18], [22] or in the series-connected multiterminal HVdc [23]–[25], the MMCs can flexibly adjust the power by regulating the dc voltage in a wide range.

However, literature on the energy storage requirement of MMCs that utilize the negative voltage capability of SMs mainly focuses on the condition of the constant rated dc voltage. In the applications of variable dc voltages, the amplitude of the energy variation also changes under different dc voltages, and its maximum does not always appear at the rated dc voltage [26], [27]. For example, if the modulation index is relatively high, the voltage ripple becomes even larger under low dc voltages than at the rated dc voltage [26], [27]. The existing optimization approaches to reduce the energy storage requirement by simply increasing the modulation index are no longer suitable for MMCs with variable dc voltages. However, limited studies explored the energy storage characteristics of MMCs with variable dc voltages. Furthermore, although an optimization approach of dynamically adjusting the dc component to allow high capacitor voltage ripples was proposed in [26], the control of capacitor voltages usually takes tens to hundreds of fundamental cycles and the high voltage ripples may also affect the lifespan of the capacitors. This condition evidently makes the MMCs with variable dc voltages less attractive.

This article proposes the analysis and optimization methods of the energy variation and energy storage requirement of MMCs with variable dc voltages. First, in Section II, an approximate analysis approach is proposed for analyzing the energy storage requirement considering the entire dc voltage range. The results reveal that when the modulation index increases and exceeds an inflection point (approximately 1.123), the energy variations under low dc voltages restrict the reduction effects on the energy storage requirement. In Section III, on the basis of the fact that the reduced fundamental-frequency ac component of the arm current under low dc voltages provides a large margin for injecting a large double-frequency circulating current, an optimal circulating current (OCC) that does not affect the maximum RMS value of the arm current is proposed to reduce the energy storage requirement in the entire dc voltage range to be close to that under the rated dc voltage. Furthermore, a practical online calculation is proposed for the required OCC in a real-time controller. In Sections IV and V, the proposed analysis and optimization methods are verified using simulation and experimental results, respectively. Finally, Section VI concludes this article.

II. Analysis of Energy Storage Requirement Under Zero or Natural Circulating Current

A. DC Voltage Range of MMCs That Contains FBSMs

Fig. 1(a) shows the topology of MMC. The arm voltages according to Kirchhoff's Law are

$$\begin{cases} u_{xp} = u_{dc}/2 - u_x \\ u_{xn} = u_{dc}/2 + u_x \end{cases} \quad (1)$$

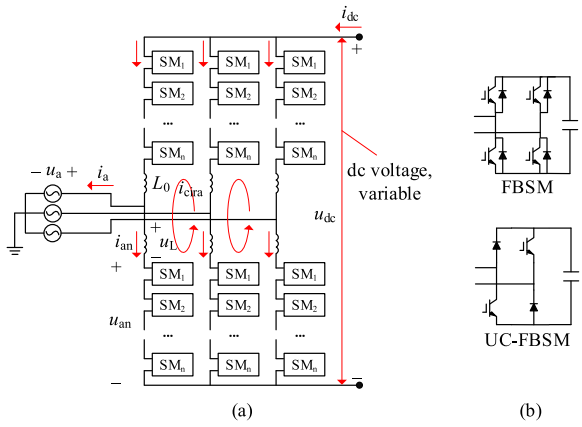

Fig. 1. Considered MMC model. (a) Topology of MMC. (b) SMs with negative voltage capability.

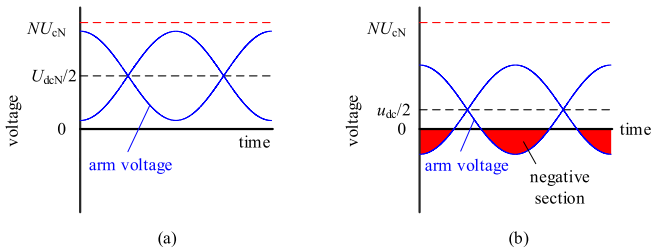

Fig. 2. Arm voltages at rated dc voltage and reduced dc voltage. (a) Rated dc voltage. (b) Reduced dc voltage.

where x = a, b, c; u_{xp} and u_{xn} are the upper and lower arm voltages of phase x; u_{dc} is the dc voltage; and u_x is the equivalent ac voltage of the converter. According to (1), the ac and dc voltages are

$$\begin{cases} u_{dc} = u_{xp} + u_{xn} \\ u_x = \frac{u_{xn} - u_{xp}}{2} \end{cases} . \quad (2)$$

The sum of the upper and lower arm voltages determines the dc voltage of the MMC, while the difference of them determines the ac voltage. If only the sum of the arm voltages varies without affecting the difference of them, as shown in Fig. 2(a) and (b), then the MMC can adjust the dc voltage without affecting the ac voltage capability. As shown in Fig. 2(b), this results in negative sections in the arm voltages. As shown in Fig. 1(b), if the MMC contains SMs that can output negative voltage levels (e.g., FB-MMC and HYB-MMC), the MMC can have adjustable dc voltage.

B. Energy Variation and Energy Storage Requirement

Given that the MMC operates symmetrically, the lower arm of phase A is taken as an example in the analysis. The arm voltage and current generate the power variation in the converter arm, expressed as

$$p_{an}(t) = u_{an}(t)\, i_{an}(t) \quad (3)$$

where $p_{\mathrm{an}}(t)$ is the power variation in the converter arm; $u_{\mathrm{an}}(t)$ is the arm voltage; and $i_{\mathrm{an}}(t)$ is the arm current, as shown in Fig. 1. The power variation then generates the energy variation $\tilde{e}\,(t)$ in the converter arm, that is,

$$\tilde{e}\,(t) = \int p_{\mathrm{an}}\,(t)\,\mathrm{d}t = \int u_{\mathrm{an}}\,(t)\,i_{\mathrm{an}}\,(t)\,\mathrm{d}t. \tag{4}$$

Then, the energy variation can be normalized [28] as

$$\tilde{e}^{*}\,(t) = \frac{\tilde{e}\,(t)}{S_{\mathrm{N}}} \tag{5}$$

where S_{N} is the rated apparent power of the MMC, and thus the unit of $\tilde{e}^{*}(t)$ is kJ/MVA. The energy variation $\tilde{e}^{*}(t)$ is a periodic function of time, and its amplitude is denoted by $\tilde{E}^{*}$. Under a certain modulation index, the value of $\tilde{E}^{*}$ is determined by the operating point (i.e., dc voltage). $\Delta E^{*}{}_{\max}$ denotes the maximum of $\tilde{E}^{*}$ in the entire operating region.

The total use of capacitor in an MMC can be evaluated using the normalized energy storage requirement in the unit of kJ/MVA [28], which is denoted by $W^{*}{}_{\mathrm{MMC}}$ and defined as

$$W^{*}_{\mathrm{MMC}} = \frac{6 \times N \times 0.5 \times C_{\mathrm{sm}} \times U^{2}_{\mathrm{cN}}}{S_{\mathrm{N}}} \tag{6}$$

where N is the number of SMs in each converter arm, C_{sm} is the SM capacitance, and U_{cN} is the rated voltage of the SM capacitor. The upper limit of the ratio of the capacitor voltage ripple is denoted by $\varepsilon_{\mathrm{lim}}$. According to Appendix A, the minimum energy storage requirement can be expressed as

$$W^{*}_{\mathrm{MMC}} = \frac{6}{(1+\varepsilon_{\mathrm{lim}})^{2}-1} \times \Delta E^{*}_{\max}. \tag{7}$$

Clearly, the energy storage requirement has a linear relationship with the maximum amplitude of the energy variation in the entire operating region, that is, $\Delta E^{*}{}_{\max}$. Therefore, the optimization problem of energy storage requirement becomes a minimization problem of the maximum amplitude $\Delta E^{*}{}_{\max}$.

Given that the amplitude of the energy variation under a certain value of dc voltage is proportional to the dc current, only the rated dc current condition is considered when determining the maximum amplitude of energy variation. This study focuses on pure active power conditions. The ac current decreases with the dc voltage because the active power declines. Aside from the fundamental-frequency ac and dc components, the arm current may also include a double-frequency circulating component. Without a special optimization strategy, the natural circulating current is typically much smaller than the dc and the fundamental-frequency ac components. Another common method is to suppress the circulating current to zero. In both scenarios, the circulating current has smaller effects on energy variation compared with those caused by the fundamental-frequency ac and dc components of the arm current. Therefore, this study excludes the effect of the circulating current to simplify the analysis. According to the deduction in Appendix B, the expression of energy variation is

$$\tilde{e}^{*}\,(t) = \tilde{e}^{*}_{1\omega}\,(t) + \tilde{e}^{*}_{2\omega}\,(t) \tag{8}$$

where $\tilde{e}^{*}_{1\omega}(t)$ and $\tilde{e}^{*}_{2\omega}(t)$ represent the fundamental- and double-frequency components of the energy variation, respectively.

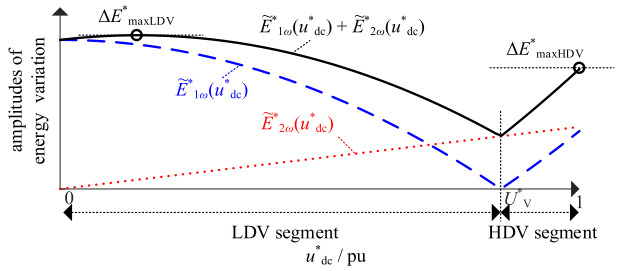

Fig. 3. Amplitudes of energy variations varying with the dc voltage under a certain value of M_0.

These components are, respectively, expressed as

$$\begin{cases} \tilde{e}^{*}_{1\omega}\,(t) = \frac{1}{3\omega}\left(\frac{M_0}{2} - \frac{u^{*2}_{\mathrm{dc}}}{M_0}\right)\sin\omega t + \frac{M_0 X^{*} u^{*}_{\mathrm{dc}}}{12\omega}\cos\omega t \\ \tilde{e}^{*}_{2\omega}\,(t) = -\frac{u^{*}_{\mathrm{dc}}}{12\omega}\sin 2\omega t - \frac{X^{*} u^{*2}_{\mathrm{dc}}}{24\omega}\cos 2\omega t \end{cases} \tag{9}$$

where ω is the angular frequency of the ac grid, X^{*} is the per-unit value of the arm inductance, and $u^{*}{}_{\mathrm{dc}}$ is the per-unit value of the dc voltage. M_0 denotes the base modulation index and is expressed as

$$M_0 = \frac{\sqrt{2}U_{\mathrm{acN}}}{U_{\mathrm{dcN}}/2} \tag{10}$$

where U_{acN} and U_{dcN} are the rated ac and dc voltages, respectively. The base modulation index M_0 represents the ac voltage normalized by the rated dc voltage and does not change with the operating points.

C. Approximate Analysis of the Maximum Amplitude of the Energy Variation

Although the energy variation is expressed in (8) and (9), obtaining the exact analytical expression of its amplitude remains difficult because the energy variation consists of the components in two frequencies. A numerical calculation based on (8) and (9) can be used to calculate the exact amplitude of the energy variation, but cannot clearly reveal how the key variables (e.g., $u^{*}{}_{\mathrm{dc}}$ and M_0) influence the amplitude of energy variation. Therefore, an approximate analysis approach is proposed, where the expressions in (9) are reasonably simplified.

The per-unit value of the arm inductance (i.e., X^{*}) is often lower than 0.2 p.u. Thus, the coefficients of the terms with X^{*} are much lower than the others in (8) and (9). The expressions are simplified by first excluding the effect of X^{*} in the approximate analysis. Then, the fundamental-frequency energy variation can be approximated as

$$\tilde{e}^{*}_{1\omega}\,(t) \approx \frac{1}{3\omega}\left(\frac{M_0}{2} - \frac{u^{*2}_{\mathrm{dc}}}{M_0}\right)\sin\omega t. \tag{11}$$

Clearly, under a certain value of M_0, the amplitude of the fundamental-frequency energy variation is a quadratic function of $u^{*}{}_{\mathrm{dc}}$, and reaches the minimum 0 when the condition of $M_0/2 - u^{*2}{}_{\mathrm{dc}}/M_0 = 0$ is fulfilled, as shown in Fig. 3. The dc voltage where the amplitude of $\tilde{e}^{*}{}_{1\omega}(t)$ reaches 0 is denoted

using $U^*_{\rm V}$ as

$$U^*_{\rm V} = \frac{M_0}{\sqrt{2}}. \tag{12}$$

Fig. 3 shows that using $U^*_{\rm V}$ as the dividing point, the entire dc voltage range can be divided into two segments, namely, high and low dc voltage segments (HDV and LDV, respectively). The amplitude of the fundamental-frequency energy variation is denoted by $\tilde{E}^*{}_{1\omega}$. If the effect of X^* is neglected, then $\tilde{E}^*{}_{1\omega}$ in the HDV and LDV segments can be approximated as

$$\tilde{E}^*_{1\omega}(u^*_{\rm dc}) \approx \begin{cases} \frac{1}{3\omega}\left(\frac{M_0}{2} - \frac{u^{*2}_{\rm dc}}{M_0}\right) & u^*_{\rm dc} < U^*_{\rm V} \\ \frac{1}{3\omega}\left(\frac{u^{*2}_{\rm dc}}{M_0} - \frac{M_0}{2}\right) & u^*_{\rm dc} \geq U^*_{\rm V} \end{cases}. \tag{13}$$

The amplitude of the double-frequency energy variation is denoted by $\tilde{E}^*{}_{2\omega}$. If the effect of X^* is neglected, then $\tilde{E}^*{}_{2\omega}$ can be approximated as

$$\tilde{E}^*_{2\omega}(u^*_{\rm dc}) \approx \frac{u^*_{\rm dc}}{12\omega}. \tag{14}$$

Fig. 3 also shows the curves of the amplitudes of the fundamental- and double-frequency energy variations when the dc voltage varies under a value of M_0. The amplitude of the fundamental-frequency energy variation, $\tilde{E}^*{}_{1\omega}(u^*{}_{\rm dc})$, first decreases and then increases with the dc voltage and has a minimum of 0 at the dividing point $U^*{}_{\rm V}$, i.e., $M_0/\sqrt{2}$. The amplitude of the double-frequency energy variation, $\tilde{E}^*{}_{2\omega}(u^*{}_{\rm dc})$, has a linear relationship with the dc voltage.

Although the amplitudes of the fundamental- and double-frequency energy variations are obtained, deriving the exact analytical expression of the amplitude of the total energy variation remains difficult because it also requires the phases of the fundamental- and the double-frequency energy variations. Another approach in the approximate analysis is to ignore the influence of phases and to directly use the sum of $\tilde{E}^*{}_{1\omega}$ and $\tilde{E}^*{}_{2\omega}$ as the amplitude of the total energy variation. Although errors may occur, this approximation can help in understanding the trend of the amplitude of the total energy variation when the dc voltage varies under different values of M_0. Furthermore, because the sum of amplitudes of the fundamental- and double-frequency components is not lower than the real amplitude of the synthesized waveform, this approach is a conservative approximation that can ensure the normal operation of MMCs.

According to (13) and (14), the approximate expression of the amplitude of the energy variation varying with $u^*{}_{\rm dc}$ is

$$\begin{aligned} \tilde{E}^*(u^*_{\rm dc}) &\approx \tilde{E}^*_{1\omega}(u^*_{\rm dc}) + \tilde{E}^*_{2\omega}(u^*_{\rm dc}) \\ &= \begin{cases} \frac{1}{3\omega}\left(-\frac{u^{*2}_{\rm dc}}{M_0} + \frac{M_0}{2} + \frac{u^*_{\rm dc}}{4}\right) & u^*_{\rm dc} \in [0, U^*_{\rm V}) \\ \frac{1}{3\omega}\left(\frac{u^{*2}_{\rm dc}}{M_0} - \frac{M_0}{2} + \frac{u^*_{\rm dc}}{4}\right) & u^*_{\rm dc} \in [U^*_{\rm V}, 1] \end{cases}. \end{aligned} \tag{15}$$

As illustrated in Fig. 3, the maximum amplitude of the energy variation in the HDV and LDV segments can be obtained, respectively, as

1) in HDV segment ($U^*{}_{\rm V} \leq u^*{}_{\rm dc} \leq 1$)

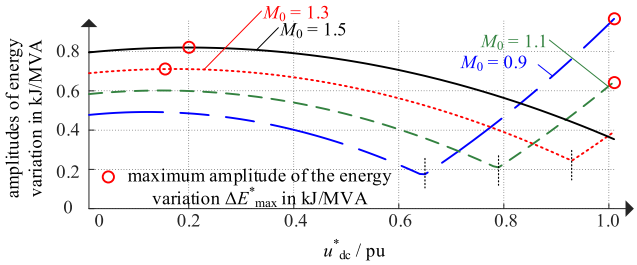

Fig. 4. Amplitudes of the energy variation in an MMC arm related to the modulation index and the dc voltage.

The HDV segment consists of high dc voltages, and the derivative of the amplitude of energy variation is

$$\frac{{\rm d}\tilde{E}^*(u^*_{\rm dc})}{{\rm d}u^*_{\rm dc}} = \frac{2}{3\omega}\left(\frac{u^*_{\rm dc}}{M_0} + \frac{1}{8}\right). \tag{16}$$

According to (16), the derivative of the amplitude of the energy variation is always greater than zero, and thus the amplitude of the energy variation increases monotonously with the dc voltage. Its maximum value appears at $u^*{}_{\rm dc} = 1.0$ p.u., which can be obtained as

$$\begin{aligned} \Delta E^*_{\rm maxHDV}(M_0) &= \frac{1}{3\omega}\left(\frac{u^{*2}_{\rm dc}}{M_0} - \frac{M_0}{2} + \frac{u^*_{\rm dc}}{4}\right)\Big|_{u^*_{\rm dc}=1} \\ &= \frac{1}{3\omega}\left(\frac{1}{M_0} - \frac{M_0}{2} + \frac{1}{4}\right). \end{aligned} \tag{17}$$

2) in LDV segment ($0 \leq u^*{}_{\rm dc} < U^*{}_{\rm V}$)

The LDV segment consists of low dc voltages, and the derivative of the amplitude of energy variation is

$$\frac{{\rm d}\tilde{E}^*(u^*_{\rm dc})}{{\rm d}u^*_{\rm dc}} = \frac{2}{3\omega}\left(-\frac{u^*_{\rm dc}}{M_0} + \frac{1}{8}\right). \tag{18}$$

The extreme point of $u^*{}_{\rm dc} = M_0/8$ can be obtained by letting (18) be equal to zero. The maximum amplitude of energy variation in the LDV segment can be obtained as

$$\begin{aligned} \Delta E^*_{\rm maxLDV}(M_0) &= \frac{1}{3\omega} \\ &\times \left(\frac{M_0}{2} - \frac{u^{*2}_{\rm dc}}{M_0} + \frac{u^*_{\rm dc}}{4}\right)\Big|_{u^*_{\rm dc}=\frac{M_0}{8}} = \frac{11M_0}{64\omega}. \end{aligned} \tag{19}$$

The maximum amplitudes of the energy variations in the HDV and LDV segments are expressed in (17) and (19), respectively. Thus, under a certain value of M_0, in the entire dc voltage range, the maximum amplitude of the energy variation can be obtained as

$$\Delta E^*_{\rm max}(M_0) = \max\left[\Delta E^*_{\rm maxHDV}(M_0), \Delta E^*_{\rm maxLDV}(M_0)\right]. \tag{20}$$

Under selected modulation indices, Fig. 4 shows the locations of $\Delta E^*{}_{\rm max}(M_0)$. According to (17), (19), (20), and Fig. 4, when the modulation index is relatively low, the maximum amplitude of energy variation is determined by $\Delta E^*{}_{\rm maxHDV}$, but when the modulation index is relatively high, the maximum amplitude of energy variation is determined by $\Delta E^*{}_{\rm maxLDV}$. This case can

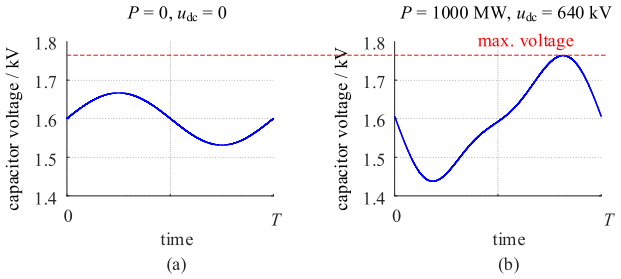

Fig. 5. Comparison of capacitor voltage ripples under $u^*_{\rm dc} = 0$ and $u^*_{\rm dc} = 1.0$ p.u. when the base modulation index is 0.8. (a) $u^*_{\rm dc} = 0$. (b) $u^*_{\rm dc} = 1.0$ p.u.

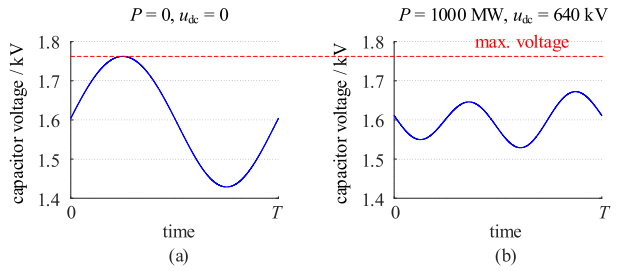

Fig. 6. Comparison of capacitor voltage ripples under $u^*_{\rm dc} = 0$ and $u^*_{\rm dc} = 1.0$ p.u. when the base modulation index is 1.4. (a) $u^*_{\rm dc} = 0$. (b) $u^*_{\rm dc} = 1.0$ p.u.

also be intuitively illustrated by the SM capacitor voltage. Fig. 5 shows the waveforms of capacitor voltage ripple under zero and rated dc voltages when the base modulation index is 0.8. The voltage ripple at the rated dc voltage is much larger than that at zero dc voltage. However, the opposite is true if the base modulation index is 1.4, as shown in Fig. 6.

Therefore, the modulation index has an inflection point, which can be calculated by establishing $\Delta E^*_{\rm maxLDV}(M_0) = \Delta E^*_{\rm maxHDV}(M_0)$ as

$$\frac{11M_0}{64} = \frac{1}{3M_0} - \frac{M_0}{6} + \frac{1}{12}. \tag{21}$$

The inflection point is the solution of (21), as

$$M_{0\_\rm inflec} = 1.123. \tag{22}$$

Then, the maximum amplitude of the energy variation under a certain value of M_0 can be expressed as

$$\Delta E^*_{\rm max}(M_0) = \begin{cases} \frac{1}{3\omega}\left(\frac{1}{M_0} - \frac{M_0}{2} + \frac{1}{4}\right) & \text{when } M_0 < M_{0\_\rm inflec} \\ \frac{11M_0}{64\omega} & \text{when } M_0 \geq M_{0\_\rm inflec} \end{cases}. \tag{23}$$

According to (23), the curve of the approximate maximum amplitude of the energy variation varying with M_0 is plotted in Fig. 7. Besides, using the numerical calculation, the exact maximum amplitude of the energy variation based on (8) and (9) considering the entire dc voltage range is also plotted in Fig. 7 for comparison. The error between the approximate and exact results is not significant. The advantage of the approximate analysis is that it not only clearly reveals the relationship between the amplitude of the energy variation and the dc voltage, but

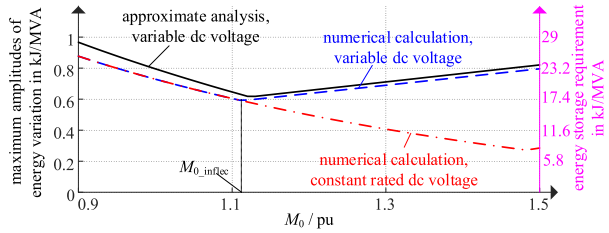

Fig. 7. Maximum amplitude of the energy variation varying with the value of M_0, and the corresponding energy storage requirements under $\varepsilon_{\rm lim} = 10\%$.

the maximum amplitude of the energy variation can also be approximated under some reasonable assumptions. With the proposed approximate analysis, how the base modulation index influences the energy storage requirement considering the entire dc voltage range can be revealed, which is indicated on the right y-axis in Fig. 7.

According to the existing studies, the amplitude of the energy variation and the energy storage requirement can be reduced greatly by increasing M_0 to about $\sqrt{2}$, if only considering the constant rated dc voltage [12], [13], [29]. However, when the variable dc voltage is considered, the amplitude of the energy variation under all possible dc voltages should be considered, and the maximum amplitude does not always appear at the rated dc voltage. Specifically, when M_0 is increased and exceeds the inflection point $M_{0\_\rm inflec}$ (approximately 1.123), the maximum amplitude of the energy variation appears at the operating points in low dc voltages, and it increases with the increase in M_0. Therefore, the reduction of the energy storage requirement by simply increasing the modulation index cannot achieve the desired effect.

The phenomenon that the amplitudes of energy variations under low dc voltages is higher than those under high dc voltages if M_0 is greater than its inflection point $M_{0\_\rm inflec}$ can also be explained with physical mechanisms. The fundamental-frequency energy variation is dominant in the total energy variation. As shown in (11), the fundamental-frequency energy variation is mainy determined by the difference between two factors. The first one, determined by the product of the dc component in the arm voltage and the fundamental-frequency component in the arm current, is proportional to the dc voltage; while the second one, determined by the product of the fundamental-frequency ac component in the arm voltage and the dc component in the arm current, is proportional to the amplitude of ac voltage. When the dc voltage decreases, the second factor remains almost unchanged, while the first one decreases accordingly. The base modulation index M_0 indicates the amplitude of the ac voltage under a given rated dc voltage. If M_0 is very high, such that the amplitude of the second factor is even greater than the difference between them at the rated dc voltage, then the amplitudes of the fundamental-frequency energy variations under low dc voltages would be higher than that under high dc voltages. Given that the fundamental-energy variation is dominant, the total energy variations under low dc voltage would also have higher amplitudes than those under high dc voltages.

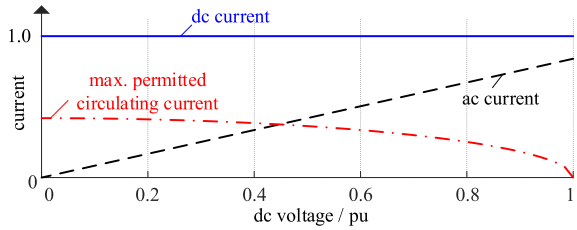

Fig. 8. Margin of the circulating current considering the RMS value of the arm current.

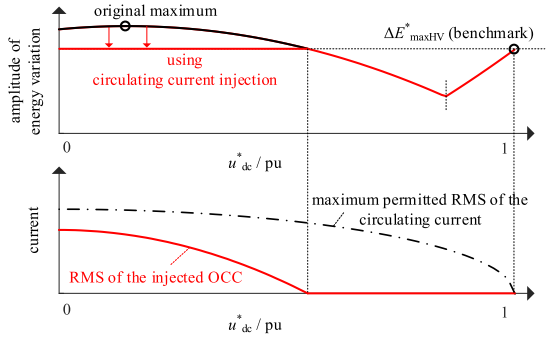

Fig. 9. Amplitude of energy variation and the corresponding optimal circulating current.

III. Optimization of Energy Storage Requirement Through Optimal Circulating Current Injection

A. Optimal Circulating Current Injection for Optimizing Energy Storage Requirement of MMCs With Variable DC Voltage

When the base modulation index exceeds the inflection point, the maximum amplitude of the energy variation appears in the low dc voltage segment, and therefore, increasing the modulation index cannot effectively reduce the energy storage requirement.

In fact, the low dc voltage also provides a large space for injecting the double-frequency circulating current to suppress the energy variation. As depicted in Fig. 8, even if the dc component of the arm current retains the rated value, the fundamental-frequency ac component of the arm current will decrease with the decrease in the dc voltage because the active power decreases. This condition makes it possible to inject large double-frequency circulating current under low dc voltages to suppress the energy variation, without increasing the maximum RMS value of the arm current.

The expression of the normalized double-frequency circulating component of the arm current is

$$i^*_{\text{cir}} = \sqrt{2} I^*_{\text{CC}} \cos\left(2\omega t - \theta_{\text{CC}}\right) \tag{24}$$

where I^*_{CC} is the RMS value of the circulating current, normalized by the rated dc current, and θ_{CC} is the initial phase. According to Appendix B, when the circulating current is taken into consideration, the expression of the energy variation is

$$\tilde{e}^*(t) = \tilde{e}^*_{1\omega}(t) + \tilde{e}^*_{2\omega}(t) + \tilde{e}^*_{3\omega}(t) + \tilde{e}^*_{4\omega}(t) \tag{25}$$

where

$$\begin{cases} \tilde{e}^*_{1\omega}(t) = \left(\frac{M_0}{6\omega} - \frac{u^{*2}_{\text{dc}}}{3\omega M_0}\right)\sin\omega t + \frac{\sqrt{2}M_0 I^*_{\text{CC}}}{4\omega}\sin(\omega t - \theta_{\text{CC}}) \\ \quad + \frac{M_0 X^* u^*_{\text{dc}}}{12\omega}\cos\omega t + \frac{\sqrt{2}M_0 X^* I^*_{\text{CC}} u^*_{\text{dc}}}{8\omega}\cos(\omega t - \theta_{\text{CC}}) \\ \tilde{e}^*_{2\omega}(t) = -\frac{u^*_{\text{dc}}}{12\omega}\sin 2\omega t + \frac{\sqrt{2}I^*_{\text{CC}} u^*_{\text{dc}}}{4\omega}\sin(2\omega t - \theta_{\text{CC}}) \\ \quad - \frac{X^* u^{*2}_{\text{dc}}}{24\omega}\cos 2\omega t - \frac{\sqrt{2}M_0^2 X^* I^*_{\text{CC}}}{8\omega}\cos(2\omega t - \theta_{\text{CC}}) \\ \tilde{e}^*_{3\omega}(t) = \frac{\sqrt{2}M_0 I^*_{\text{CC}}}{12\omega}\sin(3\omega t - \theta_{\text{CC}}) \\ \quad + \frac{\sqrt{2}M_0 X^* I^*_{\text{CC}} u^*_{\text{dc}}}{8\omega}\cos(3\omega t - \theta_{\text{CC}}) \\ \tilde{e}^*_{4\omega}(t) = -\frac{3M_0^2 X^* I^{*2}_{\text{CC}}}{16\omega}\cos(4\omega t - 2\theta_{\text{CC}}) \end{cases} \tag{26}$$

The interaction between the double-frequency circulating current and the fundamental-frequency component of the arm voltage can generate an additional fundamental-frequency energy variation. This additional energy variation can be used to counteract the original fundamental-frequency energy variation, and helps to suppress the fundamental-frequency energy variation, as shown in (25) and (26). However, the amplitude of the total energy variation is not only affected by the fundamental-frequency energy variation but is also affected by the components in other frequencies, thus complicating the optimization of the amplitude of the energy variation using circulating current.

Based on the analytical model of the energy variation, a searching approach is used to obtain the OCC. Fig. 9 illustrates that the optimization objective is considered as a problem of minimizing the maximum amplitude of the energy variation by injecting an appropriate circulating current, on the prerequisite that the RMS value of the arm current does not exceed the rated value. At the rated dc voltage, the maximum amplitude of the energy variation, $\Delta E^*_{\text{maxHDV}}$, is considered as not optimized and regarded as a benchmark. The reason is that when the dc voltage reaches the rated value, the arm current already reaches the maximum RMS value, and the permitted circulating current for reducing the energy variation is considered zero.

For each dc voltage lower than the rated value, the initial value of I^*_{CC} is first set as zero, and then the OCC is searched according to the following principles.

1) If the original amplitude of the energy variation without circulating current injection is already lower than the benchmark $\Delta E^*_{\text{maxHDV}}$, then no injection of any circulating current is necessary, and I^*_{CC} can be simply set as zero.
2) If the original amplitude of the energy variation is greater than the benchmark $\Delta E^*_{\text{maxHDV}}$, then the value of $I^*{}_{\text{CC}}$ is increased step by step (at each value of I^*_{CC}, the value of θ_{CC} also varies from $-\pi$ to π). This process continues until the resultant amplitude of energy variation becomes lower than the benchmark $\Delta E^*_{\text{maxHDV}}$.
3) If the amplitude of the energy variation is always greater than the benchmark $\Delta E^*_{\text{maxHDV}}$ even when I^*_{CC} reaches the maximum permitted value, then the problem is converted to finding the minimum amplitude of the energy variation. The prerequisite is that I^*_{CC} and θ_{CC} are in the permissible ranges.

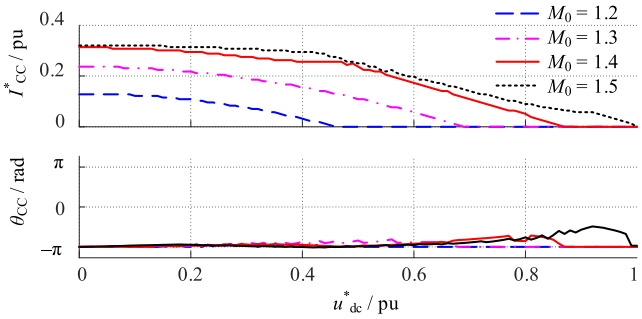

Fig. 10. Searching results of I^*_{CC} and θ_{CC} of the optimal circulating currents.

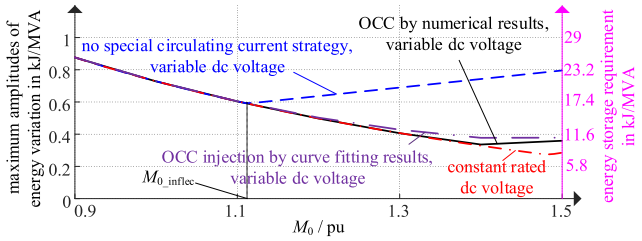

Fig. 11. Maximum amplitudes of the energy variations with the value of M_0, and the corresponding energy storage requirements under $\varepsilon_{\lim} = 10\%$.

Fig. 10 plots the curves of the RMS value I^*_{CC} and the initial phase θ_{CC} of the OCCs under several typical values of M_0. Another detail that must be noted is that, as analyzed in Section II, when M_0 is lower than M_{0_inflec} (approximately 1.123), no injection of circulating current is needed. The reason is that the original maximum amplitude of the energy variation exactly appears at the rated dc voltage. When M_0 is greater than M_{0_inflec}, the RMS value I^*_{CC} and the initial phase θ_{CC} of the OCC vary with the dc voltage.

Fig. 11 shows the comparison of the maximum amplitude of energy variation under constant rated dc voltage, under variable dc voltage without OCC injection, and under variable dc voltage with OCC injection. The corresponding energy storage requirement is indicated on the right y-axis. The comparison result shows that the proposed OCC injection has a considerable effect on the reduction of the maximum amplitude of energy variation and energy storage requirement under variable dc voltage. With OCC injection, the energy storage requirement under variable dc voltage becomes close to that under constant rated dc voltage.

B. Practical Curve-Fitting Approach in Real-Time Controller

Although the energy storage requirement of MMCs with variable dc voltage can be optimized using the proposed OCC based on the searching approach, this method is time-consuming and difficult to implement into a real-time controller in practical applications. As a simple and fast approach to calculating the required OCC in a real-time controller, a practical curve fitting approach is proposed to achieve similar results to those in Fig. 10. For the initial phase θ_{CC}, the approximation of $\theta_{CC} = -\pi$ rad is reasonable. For the RMS value I^*_{CC}, trials of several functions show that the quadratic function has the best fitting

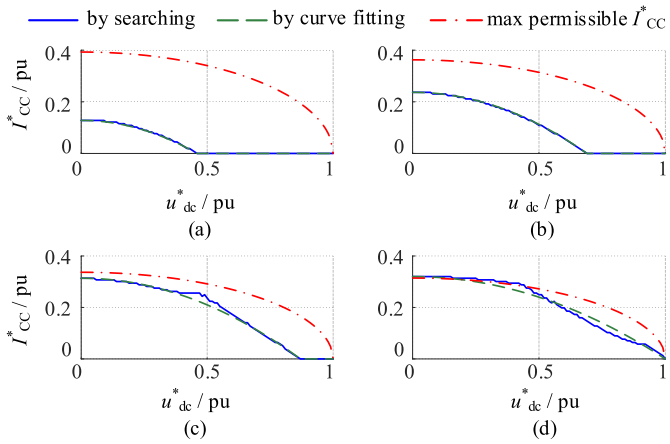

Fig. 12. Comparisons of I^*_{CC} calculated by the searching and curve-fitting approaches. (a) $M_0 = 1.2$, (b) $M_0 = 1.3$, (c) $M_0 = 1.5$, and (d) $M_0 = 1.6$.

effect, expressed as:

$$\begin{cases} I^*_{CC} = \begin{cases} K_1(M_0) \times \left(K_2(M_0) - u^{*2}_{dc}\right) & \text{when } u^*_{dc} < K_3(M_0) \\ 0 & \text{when } K_3(M_0) < u^*_{dc} \le 1, \end{cases} \\ \theta_{CC} = -\pi \end{cases} \tag{27}$$

where $K_1(M_0)$, $K_2(M_0)$, and $K_3(M_0)$ are the fitting coefficients, with values that are functions of M_0. On the basis of the numerical results, $K_1(M_0)$, $K_2(M_0)$, and $K_3(M_0)$ can be calculated using the following equations:

$$\begin{cases} K_1(M_0) = -0.938M_0 + 1.725 \\ K_2(M_0) = 2.646M_0 - 2.961 \\ K_3(M_0) = 1.8M_0 - 1.675 \end{cases}. \tag{28}$$

Fig. 12 shows the comparison of the curves of I^*_{CC} obtained by the searching and curve-fitting approaches under typical values of M_0. The results indicate that the proposed formulas have a good fitting effect, and the RMS values of the OCCs are always below the maximum permissible values. Thus, the RMS values of the arm current containing the injected OCC do not exceed the rated value. Fig. 11 shows the maximum amplitudes of the energy variation using the curve fitting OCC injection. The OCC obtained through curve fitting approach has a similar effect to that obtained through the exact searching approach, thereby allowing for implementation in a real-time controller.

Given that the proposed OCC helps to reduce the maximum amplitude of energy variation, the voltage ripples on the SM capacitors can also be suppressed. Fig. 13(a) shows the original capacitor voltage ripple when the OCC is not injected (dashed line) under a modulation index of 1.4, and the capacitor voltage ripple when the OCC controller is implemented (solid line). The comparison results show that the capacitor voltage at low dc voltage is effectively reduced, and the peak voltage under low dc voltage is equal to that under the rated dc voltage.

IV. Control Schemes

The entire controller of MMC is divided into ac, dc, and circulating current controllers, as shown in Fig. 14. When the MMC is

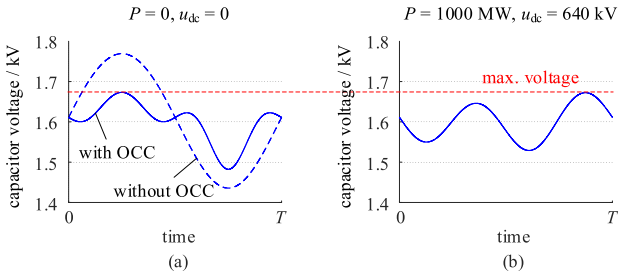

Fig. 13. Suppression effects of OCC on capacitor voltage ripples under a base modulation index of 1.4. (a) $u^*_{\rm dc} = 0$. (b) $u^*_{\rm dc} = 1.0$ p.u.

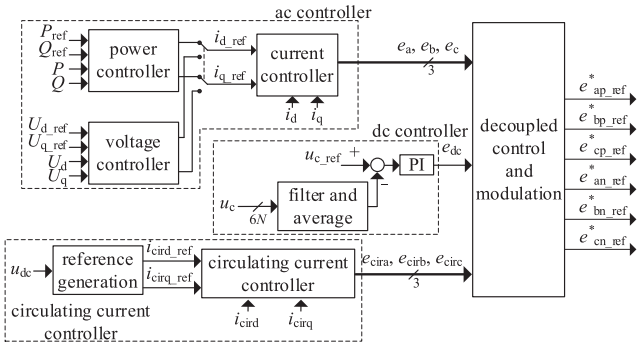

Fig. 14. Block diagram of control scheme for MMC with OCC injection under variable dc voltage.

connected with a power grid, the ac controller controls the active and reactive power; when the MMC is connected with passive loads, the ac controller controls the ac voltages. The output of the ac controller is the ac intermediate controllable voltages (ICVs) $e_{\rm a}$, $e_{\rm b}$, and $e_{\rm c}$ [30]. The capacitor voltages $u_{\rm c}$ indicate the power balance between the ac and dc sides. Therefore, the capacitor voltages are controlled to their references $u_{\rm c\_ref}$ by dynamically adjusting the dc ICV $e_{\rm dc}$ [30]. The circulating current references are calculated based on the dc voltage using (27). The output of the circulating current controller is the ICVs $e_{\rm cira}$, $e_{\rm cirb}$, and $e_{\rm circ}$ [30].

The capacitor voltages are assumed to be well balanced by the sorting and balancing algorithms. Using $u_{{\rm c}x{\rm p}}$ and $u_{{\rm c}x{\rm n}}$ to denote the capacitor voltages of the upper and lower arms of phase x, according to [30], the modulation functions can be obtained using

$$\begin{cases} e^*_{x{\rm p\_ref}} = \dfrac{(e_{\rm dc}+e_{{\rm cir}x})/2-e_x}{Nu_{{\rm c}x{\rm p}}} \\ e^*_{x{\rm n\_ref}} = \dfrac{(e_{\rm dc}+e_{{\rm cir}x})/2+e_x}{Nu_{{\rm c}x{\rm n}}} \end{cases}. \tag{29}$$

V. Simulation Results

A. Simulations of the MMC With and Without OCC Injection

A 1000-MW, ±320-kV FB-MMC is built within MATLAB/Simulink to verify the analysis of energy variation and reduction effect of the OCC on the energy storage requirement. Fig. 15 shows the diagram of the simulation, and Table I shows the simulation parameters. The base modulation index is designed as 1.4 to verify that the amplitudes of energy variations

Fig. 15. Diagram of the simulation model.

TABLE I
Parameters of Simulation

Terms	Values
Capacity (MW)	1000
Rated dc voltage (kV)	640
Rated dc current (kA)	1.5625
Rated ac voltage (kV)	549
Modulation index (M_0)	1.4
Rated SM voltage (kV)	1.6
Numbers of SMs per arm	530
Energy storage requirement (kJ/MVA)	21.49
SM capacitance (mF)	5.28

under low dc voltages are higher than those under the rated dc voltage.

In the first simulation, the circulating current is suppressed to 0. Fig. 16 shows the results. In Fig. 16(a), the dc voltage decreases from 640 to 0 kV. In the simulation, the dc current is constant and at a rated current of 1.5625 kA while the ac current varies according to the transmitted power. The active power is proportional to the dc voltage and is shown to decrease. Fig. 16(d) shows the capacitor voltages of the upper and lower arms of phase A. The low dc voltages result in high capacitor voltage ripples, which is consistent with the theoretical analysis.

In the second simulation, the proposed OCC is implemented, and the results are shown in Fig. 17. The dc voltage and the transmitted power still decrease from the rated values to 0. Fig. 17(b) shows the injection of circulating current, more of which is injected when the dc voltage is at low values but is suppressed to 0 when the dc voltage reaches 640 kV. Fig. 17(d) shows that the OCC helps to significantly reduce the capacitor voltage ripples.

B. Comparison of the Calculation and the Simulation Results of Amplitudes of Energy Variations Under Different DC Voltages

Fig. 18 shows the calculation and simulation results of the amplitude of energy variation with different dc voltages under the modulation indices of 1.2 and 1.4. In the simulation, the amplitudes of energy variation are calculated on the basis of the data output. In Fig. 18(a), where $M_0 = 1.2$, the amplitudes of energy variation under low dc voltages are optimized to be equal to the amplitude under the rated dc voltage by the OCC. In Fig. 18(b), where $M_0 = 1.4$, the amplitude of the energy variation is also optimized by the OCC. However, under certain dc voltages, the amplitudes of energy variation are still higher than that under the rated dc voltage because the circulating current has reached the maximum permitted values, and no space is available for higher OCC. The comparison between the calculation and the simulation results fits well, thereby verifying the analysis in the previous sections.

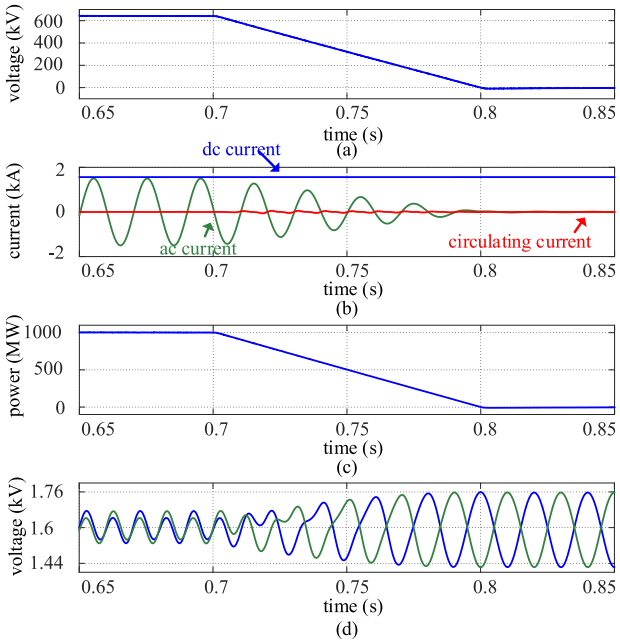

Fig. 16. Simulation result with zero circulating current. (a) dc voltage. (b) ac, dc, and circulating current. (c) transmitted active power. (d) Capacitor voltages of the upper and lower arms of phase A.

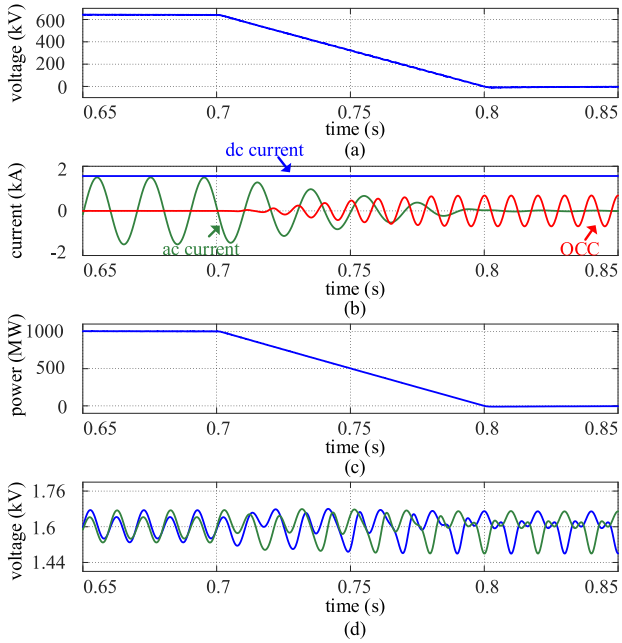

Fig. 17. Simulation result with the proposed OCC. (a) dc voltage. (b) ac, dc, and circulating current. (c) Transmitted active power. (d) Capacitor voltages of the upper and lower arms of phase A.

TABLE II
PARAMETERS OF EXPERIMENTAL PLATFORM

Terms	Values
Capacity (W)	2880
Rated dc voltage (V)	240
Rated dc current (A)	12
Rated ac voltage (V)	208
Rated SM voltage (V)	78
Numbers of SMs per arm	4
SM capacitance (mF)	1.17

C. Comparisons of the Calculation and the Simulation Results of Maximum Amplitudes of Energy Variations Under Different Modulation Indices

Fig. 19 shows the calculation and simulation results of the maximum amplitudes of energy variations under different modulation indices. The results show that the theoretical calculation and simulation results fit well, thereby verifying the analysis in the previous sections. The simulation also shows that the OCC significantly reduces the maximum amplitude of energy variation.

VI. EXPERIMENTAL RESULTS

A downscaled MMC experimental platform is built to verify the analysis of energy variation under adjustable dc voltages and to verify the effects of the proposed OCC. Four SMs are contained in each converter arm. Table II presents the parameters and Fig. 20 shows the photograph of the experimental platform.

Fig. 21(a)–(c) shows the experimental results as the circulating current is suppressed to 0. Fig. 21(a) shows the result when the dc voltage is at the rated value (240 V), and the MMC

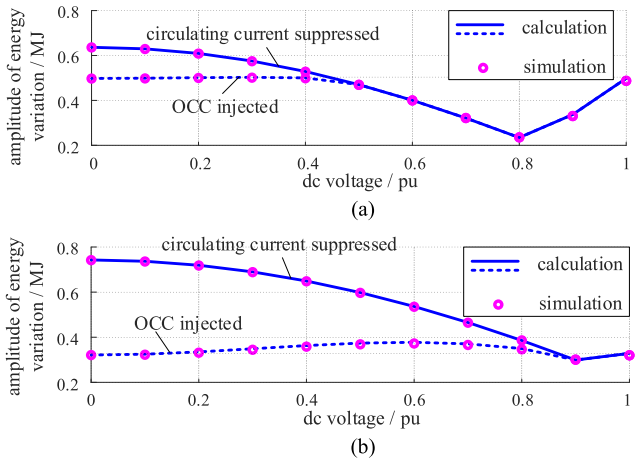

Fig. 18. Comparison of the calculation and simulation results of the amplitudes of energy variations under different dc voltages. (a) $M_0 = 1.2$. (b) $M_0 = 1.4$.

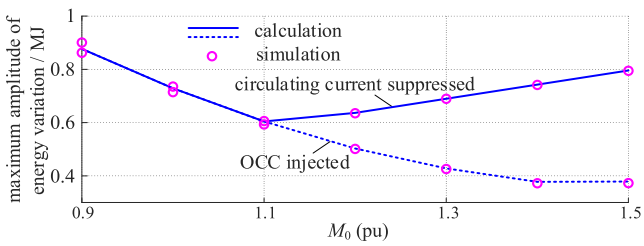

Fig. 19. Comparison of the calculation and simulation results of the maximum amplitudes of energy variations under different modulation indices.

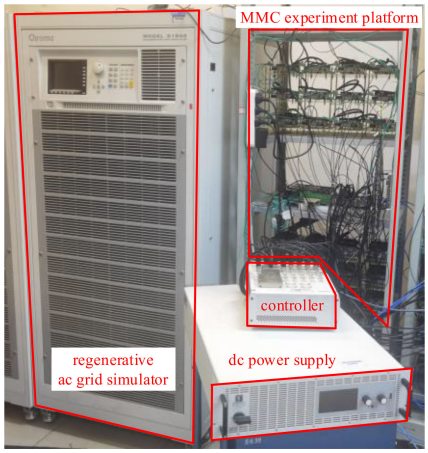

Fig. 20. Photograph of the experimental platform.

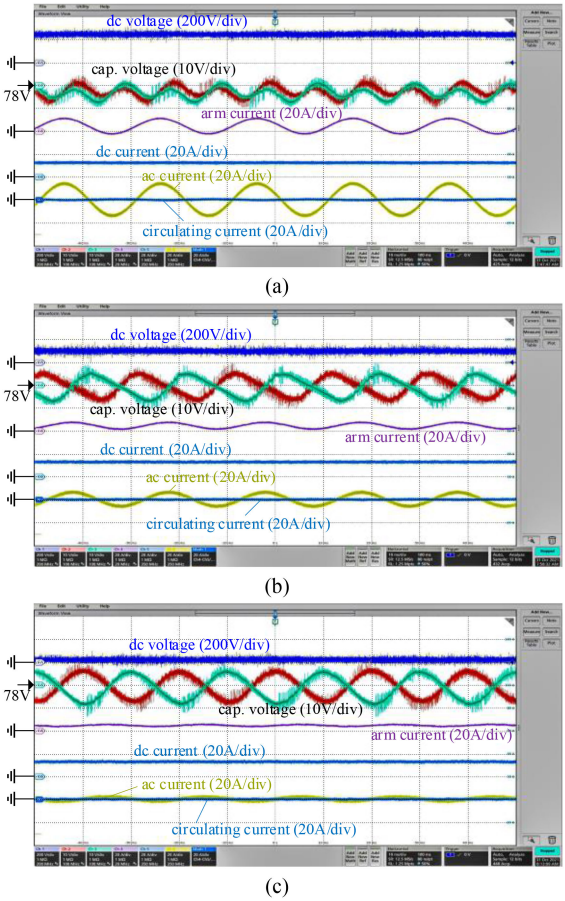

Fig. 21. Experimental results with suppressed circulating current. (a) dc voltage equals 240 V. (b) dc voltage equals 120 V. (c) dc voltage equals 0 V.

transmits the rated active power (2880 W). The fundamental-frequency variation in the capacitor voltages is almost 0, which is consistent with the analytical result. Fig. 21(b)–(c) shows the experimental results with reduced dc voltages, indicating the increasing amplitude of the capacitor voltage ripples as the dc voltage decreases.

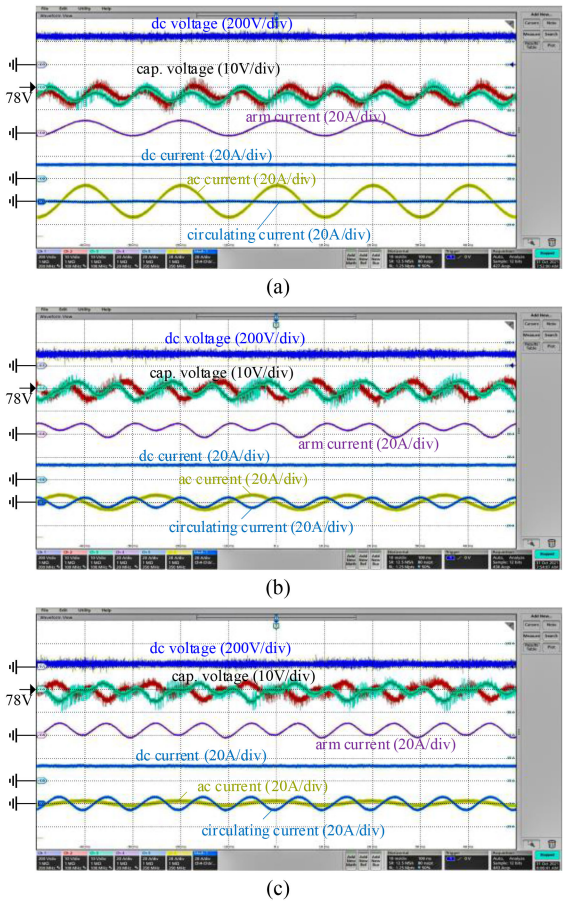

Fig. 22. Experimental results with the proposed OCC. (a) dc voltage equals 240 V. (b) dc voltage equals 120 V. (c) dc voltage equals 0 V.

Fig. 22(a)–(c) shows the experimental results as the proposed OCC injection is implemented. The amplitude of the injected circulating current increases as the dc voltage decreases. The decrease in the dc voltage does not result in a considerable increase in the amplitude of capacitor voltages. The comparison between the results in Figs. 21 and 22 indicates that the proposed OCC injection method reduces the capacitor voltage ripples in the entire dc voltage range.

VII. Conclusion

The negative voltage capability of FBSM and UC-FBSM enables the FB-MMCs, HYB-MMCs, and UC-FB-MMCs to output a wide-range adjustable dc voltage to fit special applications. Previous studies on the reduction of energy storage requirement of MMC that increases the modulation index mainly focus on the operating points of the rated dc voltage and are not suitable for MMCs with variable dc voltages. This article proposes an approach to analyze the energy variation and energy storage requirement of an MMC considering the entire dc voltage range from 0 to the rated voltage. The results indicate that when the modulation index is increased and exceeds the inflection point (approximately 1.123), the energy variation under low dc voltages restricts the reduction effects on the energy

storage requirement. Thus, simply increasing the modulation index cannot achieve the desired reduction of the energy storage requirement.

The reduced fundamental-frequency ac component of the arm current under low dc voltages provides a large margin for injecting the double-frequency circulating current. An OCC is proposed to allow the energy storage requirement that considers the entire dc voltage range to be close to that considering only the rated dc voltage. The premise is that the maximum RMS value of the arm current is not affected. Furthermore, a practical curve-fitting approach is proposed to facilitate the calculation of the required OCC in a real-time controller.

The simulation and experimental results are both consistent with the theoretical results. The simulation and experimental results also verify that the proposed optimized circulating current injection method under variable dc voltage can reduce the energy storage requirement to that under constant rated dc voltage.

Appendix A

This appendix deduces the relationship between the energy storage requirement of the MMC and the maximum amplitude of the energy variation.

The rated SM voltage is denoted as U_{cN}, and the SM capacitance is denoted as C_{sm}. Thereby, the rated energy storage in an SM capacitor is $C_{\mathrm{SM}}U^2{}_{\mathrm{cN}}/2$. The energy variation in a converter arm is denoted by $\tilde{e}(t)$. Assuming that the energy variation is evenly distributed in N SMs in a converter arm, the relationship between the capacitor voltage $u_{\mathrm{c}}(t)$ and the energy variation is expressed as

$$\frac{1}{2}C_{\mathrm{sm}}u_{\mathrm{c}}^2\left(t\right)=\frac{1}{2}C_{\mathrm{sm}}U_{\mathrm{cN}}^2+\frac{\tilde{e}\left(t\right)}{N}. \tag{A-1}$$

Solving (A-1) yields

$$u_{\mathrm{c}}\left(t\right)=\sqrt{U_{\mathrm{cN}}^2+\frac{2\tilde{e}\left(t\right)}{NC_{\mathrm{sm}}}}. \tag{A-2}$$

The upper limit of the ratio of the capacitor voltage ripple is denoted by $\varepsilon_{\mathrm{lim}}$. Therefore, the following limitation can be obtained:

$$u_{\mathrm{c}}\left(t\right)\leq\left(1+\varepsilon_{\mathrm{lim}}\right)U_{\mathrm{cN}},\forall t\in\left[0,T\right) \tag{A-3}$$

where T is the fundamental period. Substituting (A-2) into (A-3) and solving (A-3) yield

$$NC_{\mathrm{sm}}U_{\mathrm{cN}}^2\geq\frac{2\tilde{e}\left(t\right)}{\left(1+\varepsilon_{\mathrm{lim}}\right)^2-1},\forall t\in\left[0,T\right). \tag{A-4}$$

The energy storage of an MMC is defined as

$$W_{\mathrm{MMC}}=6\times\frac{1}{2}C_{\mathrm{sm}}U_{\mathrm{cN}}^2\times N. \tag{A-5}$$

Therefore, the energy storage must meet the following limitation:

$$W_{\mathrm{MMC}}^{*}\geq\frac{6\tilde{e}^{*}\left(t\right)}{\left(1+\varepsilon_{\mathrm{lim}}\right)^2-1},\forall t\in\left[0,T\right),\forall u_{\mathrm{dc}}^{*}\in\left[0,1\right] \tag{A-6}$$

where $W^{*}{}_{\mathrm{MMC}}$ and $\tilde{e}^{*}(t)$ are the normalized energy storage and energy variation in a converter arm, respectively, and their units are kJ/MVA; and $u^{*}{}_{\mathrm{dc}}$ is the per-unit value of the dc voltage.

At a certain dc voltage $u^{*}{}_{\mathrm{dc}}$, the amplitude of the energy variation is denoted by $\tilde{E}^{*}$, expressed as

$$\tilde{E}^{*}\left(u_{\mathrm{dc}}^{*}\right)=\max\left[\tilde{e}\left(t\right)\right]|_{t\in[0,T)}. \tag{A-7}$$

In the entire dc voltage range, the maximum amplitude of the energy variation is denoted by $\Delta E^{*}{}_{\mathrm{max}}$, expressed as

$$\Delta E_{\mathrm{max}}^{*}=\max\left[\tilde{E}^{*}\left(u_{\mathrm{dc}}^{*}\right)\right]\Big|_{u_{\mathrm{dc}}^{*}\in[0,1]}. \tag{A-8}$$

Thereby, substituting (A-7) and (A-8) into (A-6) yields the relationship between the energy storage requirement and the maximum amplitude of the energy variation as

$$W_{\mathrm{MMC}}^{*}=\frac{6}{\left(1+\varepsilon_{\mathrm{lim}}\right)^2-1}\times\Delta E_{\mathrm{max}}^{*}. \tag{A-9}$$

Appendix B

This appendix deduces the analytical expression of the energy variation, i.e., $\tilde{e}^{*}(t)$.

With the lower arm of phase A taken as an example, the arm current is

$$i_{\mathrm{an}}\left(t\right)=\frac{1}{3}i_{\mathrm{dc}}\left(t\right)-\frac{1}{2}i_{\mathrm{a}}\left(t\right)+i_{\mathrm{cira}}\left(t\right) \tag{B-1}$$

where i_{dc}, i_{a}, and i_{cira} are the dc current, current of phase A, and the circulating current of phase A, respectively. Variables i_{a} and i_{cira} are expressed as

$$i_{\mathrm{a}}\left(t\right)=\sqrt{2}I_{\mathrm{ac}}\cos\left(\omega t-\varphi\right) \tag{B-2}$$

$$\mathrm{i}_{\mathrm{cira}}\left(t\right)=\sqrt{2}I_{\mathrm{CC}}\cos\left(2\omega t-\theta_{\mathrm{CC}}\right) \tag{B-3}$$

where I_{ac} is the RMS value of the phase current; I_{CC} is the RMS value of the circulating current; ω is the angular frequency; φ is the power factor angle; and θ_{CC} is the initial phase of the circulating current. If only the active power is considered, then $\varphi=0$.

The arm voltage is

$$u_{\mathrm{an}}\left(t\right)=\frac{1}{2}u_{\mathrm{dc}}\left(t\right)+u_{\mathrm{a}}\left(t\right)-u_{\mathrm{L}}\left(t\right) \tag{B-4}$$

where u_{dc}, u_{a}, and u_{L} are the dc voltage, grid voltage of phase A, and the voltage that drops on the arm inductor, respectively. Variables u_{a} and u_{L} are expressed as

$$u_{\mathrm{a}}\left(t\right)=\sqrt{2}U_{\mathrm{acN}}\cos\omega t \tag{B-5}$$

$$\begin{aligned}u_{\mathrm{L}}\left(t\right)=&\frac{\sqrt{2}}{2}\omega L_0I_{\mathrm{ac}}\sin\left(\omega t-\varphi\right)\\&-2\sqrt{2}\omega L_0I_{\mathrm{CC}}\sin\left(2\omega t-\theta_{\mathrm{CC}}\right)\end{aligned} \tag{B-6}$$

where U_{acN} is the rated ac voltage and L_0 is the arm inductance.

Then, the energy variation in the converter arm is

$$\tilde{e}\left(t\right)=\int p_{\mathrm{an}}\left(t\right)\mathrm{dt}=\int u_{\mathrm{an}}\left(t\right)i_{\mathrm{an}}\left(t\right)\mathrm{dt}. \tag{B-7}$$

Substituting (B-1) and (B-4) into (B-7) yields

$$\tilde{e}\left(t\right)=\left(U_{\mathrm{dcN}}I_{\mathrm{dcN}}\right)\times\tilde{e}^{*}\left(t\right)=S_{\mathrm{N}}\times\tilde{e}^{*}\left(t\right) \tag{B-8}$$

where U_{dcN} and I_{dcN} are the rated dc voltage and current, respectively. The expression of $\tilde{e}^*(t)$ is

$$\tilde{e}^*(t) = \tilde{e}^*_{1\omega}(t) + \tilde{e}^*_{2\omega}(t) + \tilde{e}^*_{3\omega}(t) + \tilde{e}^*_{4\omega}(t) \tag{B-9}$$

where

$$\begin{cases} \tilde{e}^*_{1\omega}(t) = \left(\frac{M_0}{6\omega} - \frac{u^{*2}_{\mathrm{dc}}}{3\omega M_0}\right)\sin\omega t + \frac{\sqrt{2}M_0 I^*_{\mathrm{CC}}}{4\omega}\sin(\omega t - \theta_{\mathrm{CC}}) \\ \quad + \frac{M_0 X^* u^*_{\mathrm{dc}}}{12\omega}\cos\omega t + \frac{\sqrt{2}M_0 X^* I^*_{\mathrm{CC}} u^*_{\mathrm{dc}}}{8\omega}\cos(\omega t - \theta_{\mathrm{CC}}) \\ \tilde{e}^*_{2\omega}(t) = -\frac{u^*_{\mathrm{dc}}}{12\omega}\sin 2\omega t + \frac{\sqrt{2}I^*_{\mathrm{CC}} u^*_{\mathrm{dc}}}{4\omega}\sin(2\omega t - \theta_{\mathrm{CC}}) \\ \quad - \frac{X^* u^{*2}_{\mathrm{dc}}}{24\omega}\cos 2\omega t - \frac{\sqrt{2}M_0^2 X^* I^*_{\mathrm{CC}}}{8\omega}\cos(2\omega t - \theta_{\mathrm{CC}}) \\ \tilde{e}^*_{3\omega}(t) = \frac{\sqrt{2}M_0 I^*_{\mathrm{CC}}}{12\omega}\sin(3\omega t - \theta_{\mathrm{CC}}) \\ \quad + \frac{\sqrt{2}M_0 X^* I^*_{\mathrm{CC}} u^*_{\mathrm{dc}}}{8\omega}\cos(3\omega t - \theta_{\mathrm{CC}}) \\ \tilde{e}^*_{4\omega}(t) = -\frac{3M_0^2 X^* I^{*2}_{\mathrm{CC}}}{16\omega}\cos(4\omega t - 2\theta_{\mathrm{CC}}) \end{cases} \tag{B-10}$$

The variables in (B-10) are explained as follows: M_0 is the base modulation index; u^*_{dc} is the per-unit value of the dc voltage; I^*_{CC} is the per-unit value of I_{CC} normalized by I_{dcN}; X^* is the per-unit value of the arm inductance.

If the influence of the circulating current is neglected, then the energy variation becomes

$$\tilde{e}^*(t) = \tilde{e}^*_{1\omega}(t) + \tilde{e}^*_{2\omega}(t) \tag{B-11}$$

where

$$\begin{cases} \tilde{e}^*_{1\omega}(t) = \left(\frac{M_0}{6\omega} - \frac{u^{*2}_{\mathrm{dc}}}{3\omega M_0}\right)\sin\omega t + \frac{M_0 X^* u^*_{\mathrm{dc}}}{12\omega}\cos\omega t \\ \tilde{e}^*_{2\omega}(t) = -\frac{u^*_{\mathrm{dc}}}{12\omega}\sin 2\omega t - \frac{X^* u^{*2}_{\mathrm{dc}}}{24\omega}\cos 2\omega t \end{cases} \tag{B-12}$$

REFERENCES

[1] Y. Z. H. Rao, S. Xu, and Z. Zhu, *Research and Development of Ultra-High-Voltage VSC For the Multi-Terminal Hybrid ±800kV HVDC Project in China Southern Power Grid*. Paris, France: E-CIGRE, 2018.

[2] Y. Li, R. Cao, W. Huang, G. Li, Z. Guo, and T. Liu, "Design and simulation for the control and protection of hybrid LCC-VSC MTDC system," in *Proc. IEEE 3rd Int. Elect. Energy Conf.*, 2019, pp. 281–286, doi: 10.1109/CIEEC47146.2019.CIEEC-2019143.

[3] G. Wang, Z. Xu, and W. Hua, "Analysis on impact of Baihetan inverter connection modes on stability of Zhejiang power grid," in *Proc. IEEE Innov. Smart Grid Technol. Asia*, 2019, pp. 1075–1079, doi: 10.1109/ISGT-Asia.2019.8881179.

[4] A. Lesnicar and R. Marquardt, "An innovative modular multilevel converter topology suitable for a wide power range," in *Proc. IEEE Bologna Power Tech Conf. Proc.*, vol. 3, 2003, Art. no. 3.

[5] R. Marquardt, "Modular multilevel converter: An universal concept for HVDC-Networks and extended DC-Bus-applications," in *Proc. Int. Power Electron. Conf. ECCE ASIA*, 2010, pp. 502–507, doi: 10.1109/IPEC.2010.5544594.

[6] Y. Tang, M. Chen, and L. Ran, "A compact MMC submodule structure with reduced capacitor size using the stacked switched capacitor architecture," *IEEE Trans. Power Electron.,* vol. 31, no. 10, pp. 6920–6936, Oct. 2016, doi: 10.1109/TPEL.2015.2511189.

[7] C. Zhao, Z. Wang, Z. Li, P. Wang, and Y. Li, "Characteristics analysis of capacitor voltage ripples and dimensioning of full-bridge MMC with zero sequence voltage injection," *IEEE J. Emerg. Sel. Topics Power Electron.,* vol. 7, no. 3, pp. 2106–2115, Sep. 2019, doi: 10.1109/JESTPE.2018.2878411.

[8] K. Ilves, A. Antonopoulos, L. Harnefors, S. Norrga, L. Ängquist, and H. Nee, "Capacitor voltage ripple shaping in modular multilevel converters allowing for operating region extension," in *Proc. 37th Annu. Conf. IEEE Ind. Electron. Soc.*, 2011, pp. 4403–4408, doi: 10.1109/IECON.2011.6120033.

[9] J. Pou, S. Ceballos, G. Konstantinou, V. G. Agelidis, R. Picas, and J. Zaragoza, "Circulating current injection methods based on instantaneous information for the modular multilevel converter," *IEEE Trans. Ind. Electron.,* vol. 62, no. 2, pp. 777–788, Feb. 2015, doi: 10.1109/TIE.2014.2336608.

[10] X. Li, Q. Song, W. Liu, S. Xu, Z. Zhu, and X. Li, "Performance analysis and optimization of circulating current control for modular multilevel converter," *IEEE Trans. Ind. Electron.,* vol. 63, no. 2, pp. 716–727, Feb. 2016, doi: 10.1109/TIE.2015.2480748.

[11] Q. Tu, Z. Xu, and L. Xu, "Reduced switching-frequency modulation and circulating current suppression for modular multilevel converters," *IEEE Trans. Power Del.,* vol. 26, no. 3, pp. 2009–2017, Jul. 2011, doi: 10.1109/TPWRD.2011.2115258.

[12] L. Baruschka and A. Mertens, "Comparison of cascaded H-bridge and modular multilevel converters for BESS application," in *Proc. IEEE Energy Convers. Congr. Expo.*, 2011, pp. 909–916, doi: 10.1109/ECCE.2011.6063868.

[13] Y. Lyu, C. Li, Y. Hsieh, F. C. Lee, Q. Li, and R. Xu, "Capacitor voltage ripple reduction with state trajectory analysis for modular multilevel converter," in *Proc. IEEE Appl. Power Electron. Conf. Expo.*, 2017, pp. 1829–1836, doi: 10.1109/APEC.2017.7930947.

[14] C. Zhao et al., "Energy storage requirement optimization of hybrid modular multilevel converter with circulating current injection," *IEEE Trans. Ind. Electron.,* vol. 66, no. 9, pp. 6637–6648, Sep. 2019, doi: 10.1109/TIE.2018.2877088.

[15] G. J. M. Sousa and M. L. Heldwein, "Modular multilevel converter based unidirectional medium/high voltage drive system," in *Proc. 39th Annu. Conf. IEEE Ind. Electron. Soc.*, 2013, pp. 1037–1042, doi: 10.1109/IECON.2013.6699276.

[16] W. Yang, Q. Song, S. Xu, H. Rao, and W. Liu, "An MMC topology based on unidirectional current H-bridge submodule with active circulating current injection," *IEEE Trans. Power Electron.,* vol. 33, no. 5, pp. 3870–3883, May 2018, doi: 10.1109/tpel.2017.2722011.

[17] H. Rao et al., "Key technologies of ultra-high voltage hybrid LCC-VSC MTDC systems," *CSEE J. Power Energy Syst.,* vol. 5, no. 3, pp. 365–373, Sep. 2019, doi: 10.17775/CSEEJPES.2019.01140.

[18] H. Rao et al., "Design aspects of hybrid HVDC system," *CSEE J. Power Energy Syst.,* vol. 7, no. 3, pp. 644–653, May 2021, doi: 10.17775/CSEEJPES.2020.00980.

[19] Q. Song, S. Xu, Y. Zhou, Y. Gim, Z. Li, and Z. Deng, "Active fault-clearing on long-distance overhead lines using a hybrid modular multilevel converter," in *Proc. IEEE 28th Int. Symp. Ind. Electron.*, 2019, pp. 2033–2038, doi: 10.1109/ISIE.2019.8781312.

[20] T. Bandaru, D. Samajdar, P. B. S. Varma, T. Bhattacharya, and D. Chatterjee, "Optimum injection of second harmonic circulating currents for balancing capacitor voltages in hybrid MMC during reduced DC voltage conditions," *IEEE Trans. Ind. Appl.,* vol. 56, no. 2, pp. 1649–1660, Mar./Apr. 2020, doi: 10.1109/TIA.2020.2967277.

[21] J. Hu, Z. He, L. Lin, K. Xu, and Y. Qiu, "Voltage polarity reversing-based DC short circuit FRT strategy for symmetrical bipolar FBSM-MMC HVDC system," *IEEE J. Emerg. Sel. Topics Power Electron.,* vol. 6, no. 3, pp. 1008–1020, Sep. 2018, doi: 10.1109/JESTPE.2018.2820076.

[22] G. Li et al., "Power reversal strategies for hybrid LCC/MMC HVDC systems," *CSEE J. Power Energy Syst.,* vol. 6, no. 1, pp. 203–212, Mar. 2020, doi: 10.17775/CSEEJPES.2019.01050.

[23] Z. Li, Q. Song, R. Zeng, B. Zhao, J. Meng, and Z. Deng, "A DC grid access solution based on series-connected distributed full-bridge submodule-based MMCs," in *Proc. IEEE 28th Int. Symp. Ind. Electron.*, 2019, pp. 697–701, doi: 10.1109/ISIE.2019.8781208.

[24] G. Guo et al., "Series-connected-based offshore wind farms with full-bridge modular multilevel converter as grid- and generator-side converters," *IEEE Trans. Ind. Electron.,* vol. 67, no. 4, pp. 2798–2809, Apr. 2020, doi: 10.1109/TIE.2019.2912777.

[25] G. Guo et al., "HB and FB MMC based onshore converter in series-connected offshore wind farm," *IEEE Trans. Power Electron.,* vol. 35, no. 3, pp. 2646–2658, Mar. 2020, doi: 10.1109/TPEL.2019.2929689.

[26] W. Yang, Q. Song, and B. Zhao, "Energy storage requirement and low capacitance operation of unidirectional current H-bridge modular multilevel converters," *IEEE Trans. Power Electron.,* vol. 34, no. 12, pp. 11748–11759, Dec. 2019, doi: 10.1109/TPEL.2019.2910456.

[27] X. Yu, Y. Wei, and Q. Jiang, "New submodule circuits for modular multilevel current source converters with DC fault ride through capability," in *Proc. IEEE Appl. Power Electron. Conf. Expo.*, 2016, pp. 1468–1474, doi: 10.1109/APEC.2016.7468062.

[28] K. Ilves, S. Norrga, L. Harnefors, and H. Nee, "On energy storage requirements in modular multilevel converters," *IEEE Trans. Power Electron.,* vol. 29, no. 1, pp. 77–88, Jan. 2014, doi: 10.1109/TPEL.2013.2254129.

[29] Q. Song, W. Yang, B. Zhao, S. Xu, H. Rao, and Z. Zhu, "Energy storage requirement reduction using negative voltage states of a full-bridge modular multilevel converter," *IEEE Trans. Power Electron.,* vol. 34, no. 6, pp. 5243–5255, Jun. 2019, doi: 10.1109/tpel.2018.2869464.

[30] W. Yang, Q. Song, and W. Liu, "Decoupled control of modular multilevel converter based on intermediate controllable voltages," *IEEE Trans. Ind. Electron.,* vol. 63, no. 8, pp. 4695–4706, Aug. 2016, doi: 10.1109/TIE.2016.2549001.

Zhengxuan Li (Student Member, IEEE) was born in Beijing, China, in 1995. He received the B.S. degree in electrical engineering from North China Electric Power University, Beijing, China, in 2018. He is currently working toward the Ph.D. degree in electrical engineering with Tsinghua University, Beijing, China.

His research interests include modular multilevel converter, wind power, and VSC-HVdc transmission system.

Qiang Song (Senior Member, IEEE) was born in Changchun, China, in 1975. He received the B.E.E. and Ph.D. degrees in electrical engineering from Tsinghua University, Beijing, China, in 1998 and 2003, respectively.

From 2003 to 2008, he was a Lecturer with the Department of Electrical Engineering, Tsinghua University, where he has been an Associate Professor, since 2008. His research interests include high-power electronic interfaces for utility system, flexible ac transmission system, VSC-HVdc system, and custom power quality.

Shukai Xu (Senior Member, IEEE) received the B.E. and Ph.D. degrees in electrical engineering from Tsinghua University, Beijing, China, in 2002 and 2007, respectively.

He is currently the Deputy Director of Innovation Department of China Southern Power Grid, Guangzhou, China. His research interests include FACTS and VSC-HVdc.

Biao Zhao (Senior Member, IEEE) was born in Hubei, China, in 1987. He received the B.S. degree in electrical engineering from the Department of Electrical Engineering, Dalian University of Technology, Dalian, China, in 2009, and the Ph.D. degree in electrical engineering from the Department of Electrical Engineering, Tsinghua University, Beijing, China, in 2014.

He is currently an Associate Professor with the Department of Electrical Engineering, Tsinghua University. His research interests include high-power converters, high-power semiconductor devices, and flexible dc transmission and distribution systems.

Dr. Zhao is a Senior Member of the Chinese Society for Electrical Engineering and the Chinese Electro-Technical Society.

Zhanqing Yu (Member, IEEE) was born in Inner Mongolia, China, in 1981. He received the B.Sc. and Ph.D. degrees in electrical engineering from the Department of Electrical Engineering, Tsinghua University, Beijing, China, in 2003 and 2008, respectively.

He was a Postdoctoral Researcher, Lecturer, and Associate Professor with the Department of Electrical Engineering, Tsinghua University, in 2008, 2010, and 2012, respectively. He has participated in several projects sponsored by High-Tech R&D Program (863 Program), National Basic Research Program of China (973 Program), and National Natural Science Foundation of China. His research interests include dc grid, dc breaker, electromagnetic environment, electromagnetic compatibility, and lightning protection.

Rong Zeng (Senior Member, IEEE) was born in Shaanxi, China, in 1971. He received the B.Eng., M.Eng., and Ph.D. degrees in electrical engineering from the Department of Electrical Engineering, Tsinghua University, Beijing, China, in 1995, 1997, and 1999, respectively.

He was a Lecturer, an Associate Professor, and a Professor with the Department of Electrical Engineering, Tsinghua University, in 1999, 2002, and 2007, respectively. His research interests include air gap discharge, lightning protection, and electromagnetic compatibility in power systems, electric and magnetic field measurement by integrated electro-optical sensors, power semiconductor, HVdc system, and direct current circuit breaker.